ORIGINAL PAPER

Artificial neural network-based meta-models for predicting the aerodynamic characteristics of two-dimensional airfoils for small horizontal axis wind turbine

Neeraj Verma[1] · Beena D. Baloni[1]

Abstract

Blade element momentum theory is extensively used to design and characterize the performance of the wind turbine. Aerodynamic characteristics of the airfoils used in the blades of the wind turbine are one of the crucial parameters of the blade element momentum theory. The aerodynamic characteristics of airfoil can be significantly influenced by Reynolds number besides the angle of attack. Thus, an inadequate consideration of Reynolds number for aerodynamic characteristics of the airfoil can result in discrepancy in the optimum design and performance evaluation capability of the blade element momentum theory. Several mathematical models, and semi-empirical relations to parameterize the aerodynamic characteristics of two-dimensional airfoil in blade element momentum theory, inherently lack dependency on Reynolds number and thus open a scope for uncertainty. An artificial neural network-based model is proposed to predict the lift and drag coefficient of airfoil as a function of not only the angle of attack but also the Reynolds number. A series of six in-house developed airfoils for small wind turbine have been considered for the present study. The computational fluid dynamic results of the airfoil with a range of Reynolds number (100,000–2,000,000) and angle of attack (0°–20°) were utilized to develop the model. A high coefficient of determination and low root-mean-square error of the developed models for a test dataset suggests the robust capabilities and effective topology of the artificial neural network-based model to predict the lift and drag coefficient of the airfoils with respect to a given angle of attack and Reynolds number. The developed model can then be used to replace the traditional analytical or semi-empirical model for mathematical representation of airfoil in the blade element momentum theory and thus reduce the uncertainty on account of inadequate consideration of Reynolds number for aerodynamic characteristics of airfoil in design and performance evaluation.

✉ Neeraj Verma
    turbo.neeraj@gmail.com

1   Department of Mechanical Engineering, Sardar Vallabhbhai
    National Institute of Technology, Surat, India

Graphic abstract

(comparative data for one of the six airfoils for small horizontal axis wind turbine)
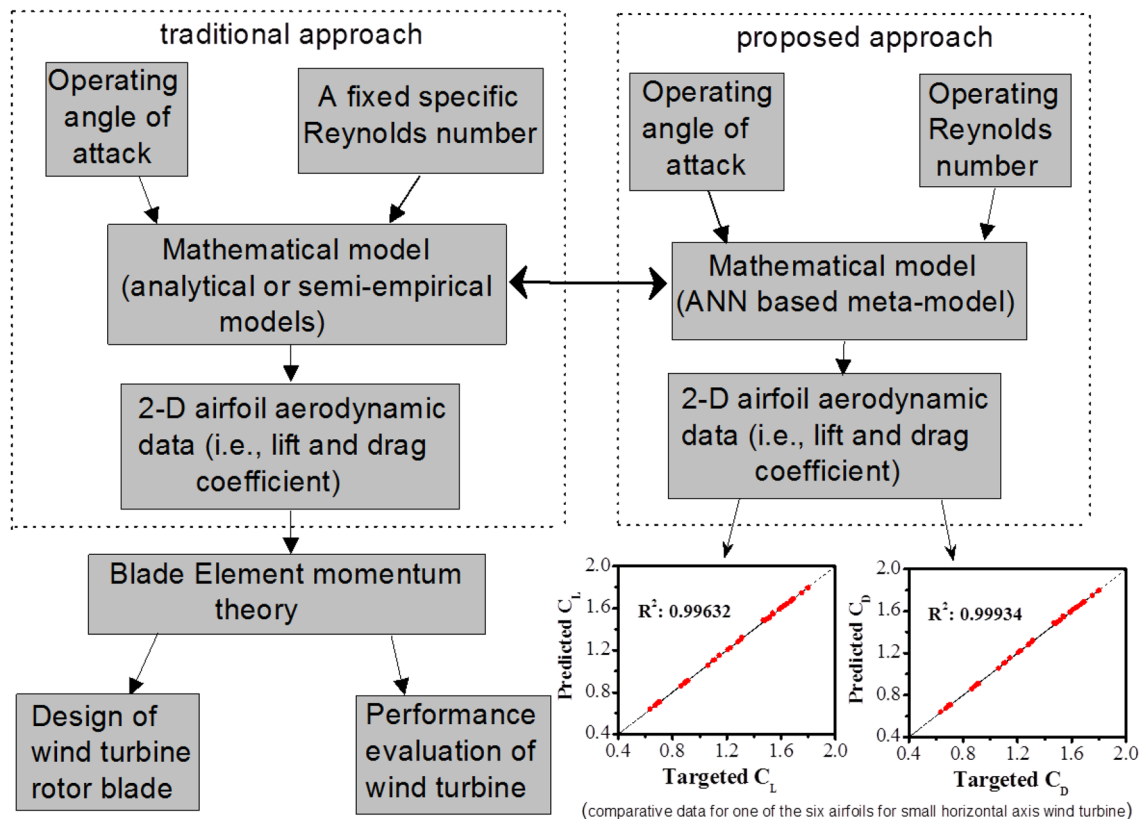
Keywords Blade element momentum theory · Aerodynamic characteristics · Artificial neural network · Airfoils · Meta-model · Computational fluid dynamics

Introduction

For the aerodynamic design and performance evaluation of the wind turbine, various computational approaches such as blade element momentum (BEM) theory (Hassanzadeh et al. 2016), vortex wake method (Chattot 2003) and computational fluid dynamic (CFD) (Bai and Wang 2016) have been developed. However, the blade element momentum theory, due to its simplicity and accuracy, is widely used amongst scientific and industrial communities (Lanza-fame and Messina 2007). Blade element theory requires the division of blade into multiple sections. The aerodynamic forces on each section are calculated by assuming the aerodynamic forces acting on two-dimensional airfoils subjected to local flow conditions, and thus the thrust and torque acting on the blade are obtained. Thus, the performance evaluation of a wind turbine blade is greatly dependent on the aerodynamic characteristics of the two-dimensional airfoil subjected to local flow conditions. Moreover from a design aspect, which primarily deals with

determining the optimum chord and twist distribution, the aerodynamic characteristics of the two-dimensional airfoil play a crucial role in the aerodynamic design of wind turbine rotor blade. El-Okda (2015) had compared various chord distribution models which primarily depends on the aerodynamic characteristics of the two-dimensional airfoil.

Since the design and performance evaluation of the wind turbine rotor blade is significantly dependent on the two-dimensional airfoil aerodynamic data, it is imperative to account for the factors that may influence the aerodynamic performance of the airfoils. The aerodynamic characteristics of two-dimensional airfoil, besides depending on the angle of attack, Reynolds number also had a significant influence on the aerodynamic characteristics of the airfoils (Zhu et al. 2014). Although the studies accounting the angle of attack are widely covered in conjunction to studies with blade element momentum theory, the studies with Reynolds number largely remains limited. Ceyhan (2012) investigated the influence of very high Reynolds number on the rotor design and performance,

and suggested that at higher Reynolds number considerations, a rotor design with up to 20% reduction in chord can be achieved as a result of increase in lift coefficient and decrease in drag coefficient. MaTavish et al. (2013) experimentally investigated the influence of Reynolds number on the thrust coefficient and near wake influence for a small-scale wind turbine and the results indicates that wake expansion and thrust coefficient may not match the scaled version of the same rotor, suggesting the influence of Reynolds number. Ge et al. (2015) studied the influence of Reynolds number on the aerodynamic design of a wind turbine and suggested that a wind turbine design using airfoil data base with mismatch in Reynolds number from the actual one may result in an incorrect estimation of load and annual energy prediction. Miller et al. (2019) investigated the power and thrust coefficient of a scaled turbine model as a function of Reynolds number in a specialized compressed air wind tunnel and observed a strong dependency of power coefficient with Reynolds number.

Despite the experimental studies suggesting the significance of Reynolds number, the numerical studies with blade element momentum theory has been largely limited to a range of specific Reynolds number which may not exactly corresponds to the actual variation of Reynolds number on the rotor blades. Bai et al. (2017), suggested average Reynolds number distribution for the entire length of the blade, obtained by considering average chord distribution. Although strategy has been devised to account the local Reynolds number variation along the length of the blade in the blade element momentum theory for integrated design and performance evaluation (Wang et al. 2012), a lack of attempts to investigate the local variation of Reynolds number attributes to the inadequate mathematical representation of two-dimensional airfoil data. For the mathematical representation of the two-dimensional airfoil aerodynamic data, various analytical or semi-empirical methodologies have been proposed. Lanzafame and Messina (2007) implemented a fifth-order logarithmic polynomial equation to fit lift and drag coefficient of S809 airfoil for angle of attack ranging from −6° to 20°. Bavanish and Thyagarajan (2013) have suggested different linear equations to represent the lift coefficient for symmetric and circular arc airfoils. Bai et al. (2016) utilized a second-order and third-order polynomial equations to represent lift and drag coefficient of S822 and S823 airfoils for angle of attack less than stall angle, respectively. Other linear, nonlinear, lookup tables and direct curve fitting techniques to represent the aerodynamic characteristics of airfoils are also discussed (Leishman 2006).

Although the above-mentioned analytical or semi-empirical methodologies provide qualitatively correct results, however, due to inherent difficulty in modeling highly nonlinear aerodynamic phenomenon near to stall angles, as well as the frequent need to interpolate between the population of aerodynamic data obtained through different mediums and lack of dependency on Reynolds number, the numerical results are quite unreliable. An aerodynamic module based on artificial neural network (ANN) may offer certain advantages as it utilizes the results of the training set by means of adequately trained and validated neural networks. In recent years, ANN had shown its capability to effectively predict the behavior of complex and non-linear system (Gue et al. 2020). It basically comprises of an input layer that receives data, a hidden layer that processes the data, and an output layer that sends the computed information. These layers have the capability to learn, memorize and establish a relationship between inputs and outputs and thus make ANN a better alternative to empirical model (Wallach et al. 2006).

In the present work, in an effort to contribute to the research on the influence of Reynolds number on the design and performance evaluation of the wind turbine rotor, adequate mathematical model to represent the two-dimensional airfoil data as a function of not only the angle of attack but also the Reynolds number is proposed. An ANN-based meta-model is proposed, which would provide the necessary lift and drag coefficient of the airfoil at a given Reynolds number and angle of attack, to be utilized in the blade element momentum theory for design and performance evaluation of the wind turbine rotor blade, as shown in Fig. 1 and thus reducing the uncertainty in optimum design and performance evaluation on account of inadequate consideration of Reynolds number. The ongoing in-house research on small wind turbine has been utilized for the present work. A series of six in-house developed airfoils, namely SV1, SV2, SV3, SV4, SV5, and SV6, encompassing a range of geometric attributes has been utilized and thus also attempting to develop a comprehensive scheme. The meta-models based on ANN has been developed for each airfoil which are capable of predicting the lift and drag coefficient of the airfoil under consideration over a range of Reynolds number (100,000–2,000,000) and also over a range of angle of attack (0°–20°). To train the ANN models, the necessary dataset has been obtained from the numerical simulation of the airfoils. One of the key challenges in developing the ANN model is establishing the adequate topology i.e., the number of layers, number of neurons and adequate activation functions. Through this work an adequate topology for the ANN models for describing the lift and drag coefficient of the airfoils as function of Reynolds number and angle of attack is also suggested.

Materials and methods

The development of ANN-based meta-models to predict the lift and drag coefficient of the concerned airfoils for a given range of Reynolds number and angle of attack begins
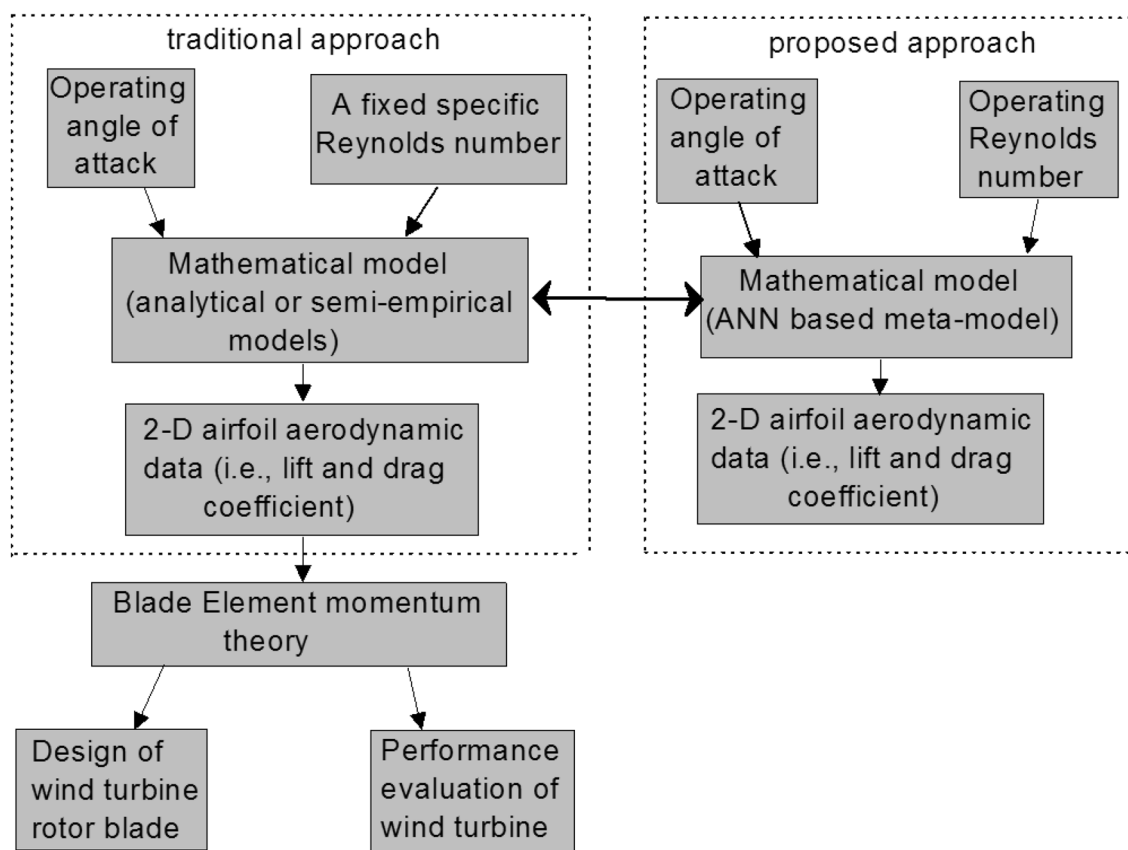
Fig. 1 Proposed ANN-based meta-model in blade element momentum theory

with generating a training dataset. The training dataset comprises of the lift and drag coefficient of the airfoils at a given Reynolds number and angle of attack, obtained by numerical simulation of the airfoils. With the training dataset, a suitable topology of the ANN which describes the number of hidden layers, neurons and activation function is obtained by trial and error method. Finally, the developed models were validated with a set of test dataset which had not been utilized in the training of the model.

Airfoils

The airfoils under consideration, i.e., SV1, SV2, SV3, SV4, SV5 and SV6 are in-house developed airfoils for its application in small horizontal axis wind turbine. The airfoils under consideration extend over a range of thin to thick airfoils. Generally, an airfoil with maximum thickness in the range of $0.11c$ to $0.15c$ is categorized as thin airfoils, whereas the airfoils with maximum thickness in the range of $0.16c$ to $0.21c$ is categorized as thick airfoils (Tangler and Somers 1995). The maximum thickness and maximum camber of the given airfoils ranges from $0.2091c$ to $0.1035c$ and $0.0864c$ to $0.0673c$, respectively, where c is the chord length of the airfoil. This given range of maximum thickness and maximum

camber signifies the diversity of the airfoils. Figure 2 shows the graphical representation of the given airfoils. Table 1 shows the geometric features of the given airfoils.

Numerical simulation

The numerical simulations of the airfoils were carried out using commercially available CFD code ANSYS® Fluent (2013). For the numerical simulation, a general-type computational case was formulated, comprising of computational domain with C–H topology, which extends from $25c$ in downstream to $15c$ in the upstream. For the analysis, $SSTk - \omega$ turbulence model along with coupled pressure velocity coupling scheme was employed (Reggio et al. 2011). The adequate mesh elements for the computational domain were obtained by grid independence test. For the precise simulation of the boundary layer, Y+, a non-dimensional distance from the wall to first node of the mesh, is suggested to be less than 1 (Belamadi et al. 2016). However to account for the change in the Reynolds number during the analysis over the range of operating conditions, variation of lift and drag coefficient was observed with change in the average Y+ and an adequate first layer height of the mesh elements was obtained. For the validation of the numerical
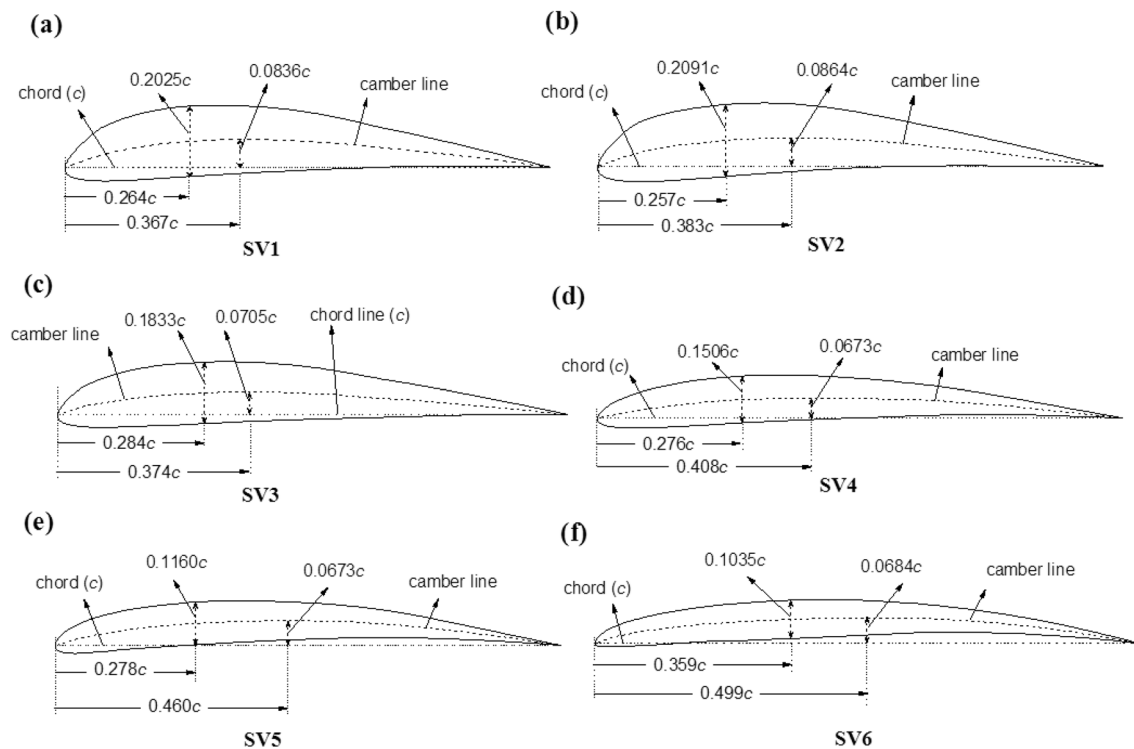
Fig. 2 Schematic view of in-house developed airfoils

Table 1 Geometric features of the in-house developed airfoils

Airfoil	Maximum thickness	Position	Maximum camber	Position
SV1	$0.2025c$	$0.264c$	$0.0836c$	$0.367c$
SV2	$0.2091c$	$0.257c$	$0.0864c$	$0.383c$
SV3	$0.1833c$	$0.284c$	$0.0705c$	$0.374c$
SV4	$0.1506c$	$0.276c$	$0.0673c$	$0.408c$
SV5	$0.1160c$	$0.278c$	$0.0673c$	$0.460c$
SV6	$0.1035c$	$0.359c$	$0.0684c$	$0.499c$

simulation, due to the lack of the experimental results, the above-mentioned formulated computational case was utilized for the numerical simulation of range of airfoil, i.e., S809, NACA 4412 and E387, over a range of operating conditions. The numerical results of these airfoils were then compared with experimental results obtained from literature at corresponding operating conditions to assess the robust capability of the formulated computational case.

The numerical simulation of the S809 airfoil was utilized to determine the adequate mesh elements and their first layer height. The domain and mesh generation was performed using the commercially available tool ANSYS® ICEM-CFD (2015). Figure 3a-b shows the variation of lift and drag coefficient with change in mesh elements. From

Fig. 3a, b it can be observed that after 29,452 mesh elements, the lift and drag coefficient seems to be independent of mesh elements. From Table 2, the lift and drag coefficient corresponding to 59,466 mesh elements changes by 0.08% and −0.07% with respect to lift and drag coefficient corresponding to 29,452 mesh elements, respectively. However, with a conservative approach, 116,216 elements with difference in lift and drag coefficient of −0.05% and −0.14% with respect to lift and drag coefficient corresponding to previous mesh elements (i.e., 59,466 mesh elements), were adopted for further analysis. Figure 3c-d shows the variation of lift and drag coefficient with average Y+ and is also tabulated in Table 3. From Fig. 3c-d it can be observed that up to an average Y+ of 1.61, the lift and drag coefficient is more or less remains the same. Thus to ensure the average Y+ does not exceed the 1.61 during the numerical simulations over the range of Reynolds number, the first layer height (0.00002 m) of the mesh elements corresponding to a conservative Y+ of 0.48 is chosen. Figure 4 shows the comparison of the numerical results and the experimental results at corresponding operating conditions for S809, NACA 4412 and E387 airfoils, which also demonstrate the capability of the formulated computational case to produce results with qualitatively fair degree of agreement with the experimental results.
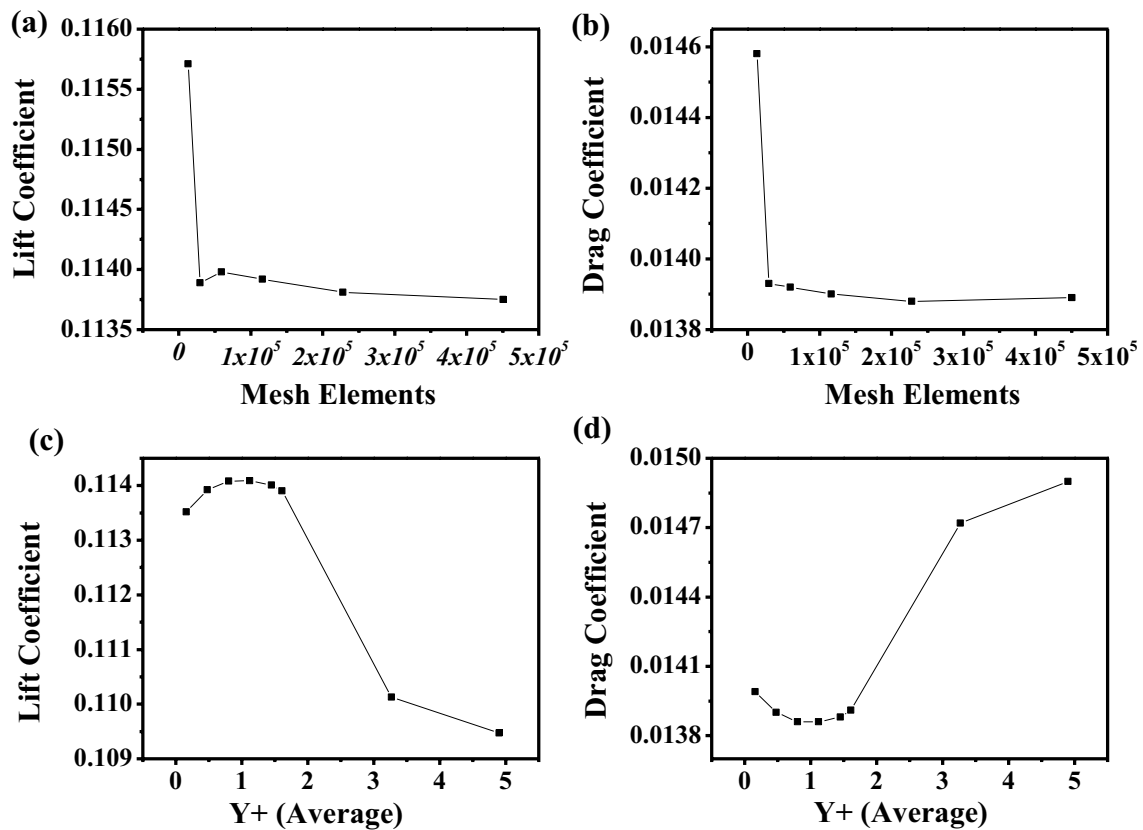
Fig. 3 Grid Independence test and average Y+ variation test **a** lift coefficient versus mesh elements, **b** drag coefficient versus mesh elements, **c** lift coefficient versus Y+ (average), and **d** drag coefficient versus Y+ (average)

Table 2 Various ANN models based on the number of neurons

Mesh elements	Lift coefficient	Difference (in%)	Drag coefficient	Difference (in %)
13,156	0.11571	–	0.01458	–
29,452	0.11389	− 1.57	0.01393	− 4.46
59,466	0.11398	0.08	0.01392	− 0.07
116,216	0.11392	− 0.05	0.0139	− 0.14
228,165	0.11381	− 0.10	0.01388	− 0.14
450,660	0.11375	− 0.05	0.01389	0.07

Table 3 Lift and drag coefficient variation with average Y+

Y+ (average)	Lift coefficient	Drag coefficient
0.16	0.11352	0.01399
0.48	0.11392	0.0139
0.8	0.11408	0.01386
1.12	0.11409	0.01386
1.45	0.11401	0.01388
1.61	0.1139	0.01391
3.27	0.11013	0.01472
4.9	0.10947	0.0149

Artificial neural network (ANN)

There are varieties of ANN models available; however, among them, the multilayered perceptron (MLP) networks with back propagation training algorithm is the most popular network for prediction purposes (Behera et al. 2015). Generally, a MLP structure is characterized by a network of input layer, hidden layer, and output layer with each layer consisting of different number of processing elements, also known as neuron (Chakraborty et al. 2013). For the present work, the inputs comprises of two operating parameters, i.e.,
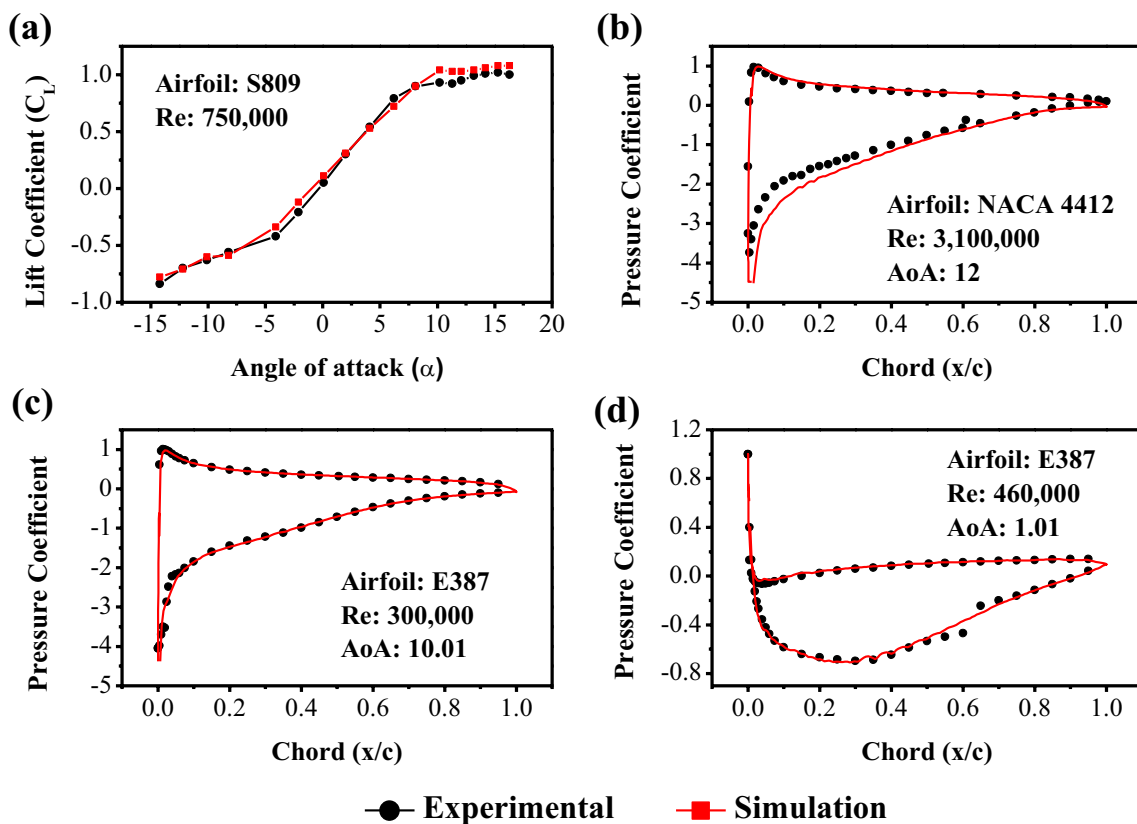
Fig. 4 Comparison of numerical simulation and experimental results for **a** S809 (Hand et al. 2001), **b** NACA 4412 (Pinkerton 1936), **c** E387 (McGhee et al. 1988) and **d** E387 (McGhee et al. 1988)

Reynolds number and angle of attack, whereas the outputs comprises of aerodynamic characteristics, i.e., lift and drag coefficients. Thus, each input and output layer has two neurons, respectively. The input and output are linked to each other through the hidden layer and the output layer. The input and output layer has fixed two neurons, whereas the hidden layer has a different number of neurons for different cases and thus results in various ANN models.

The input signal (X_i), i.e., the Reynolds number and the angle of attack, are generally scaled (x_i), as given by Eq. (1), are perceived by the input neurons. The weighted input signal (x) i.e., synaptic weight times the output of the input neuron and coupled with a bias are processed through a sigmoidal (tansig) transfer function, as given by Eq. (2), in the hidden layer. The weighted output from the hidden layer, i.e., the synaptic weight associated with neuron at output layer times the output from the neuron at the hidden layer, coupled with bias are perceived by the neurons of the output layer and are also processed with sigmoidal transfer function in the output layer. Finally, the output signals from the output layer are received by the output neurons. The output signals (C_h) from the output neurons are later again scaled (c_h), given by Eq. (3), to produce the predicted aerodynamic characteristics, i.e., lift and drag coefficients.

$$x_i = \frac{2(X_i - X_{\min})}{(X_{\max} - X_{\min})} + 1 \tag{1}$$

$$\text{tansig}(x) = \frac{2}{1 + e^{-2x}} - 1 \tag{2}$$

$$c_h = \left(\frac{C_{\max} - C_{\min}}{2}\right)(C_h + 1) + C_{\min} \tag{3}$$

where, $X_{\min}$ and $X_{\max}$ represents the minimum and maximum of the input signal, whereas $C_{\min}$ and $C_{\max}$ represent the minimum and maximum of the output signal.

$$\text{MSE} = \frac{1}{n} \sum_{m=1}^{n} \left(Y_{m,\text{actual}} - Y_{m,\text{output}}\right)^2 \tag{4}$$

Due to the unidirectional nature of signal flow from input to output neuron, the network is known as the feed-forward network. The errors are calculated by comparing the data from the output layer with the original target data. The weight and bias of each neuron in the hidden and output layers are updated based on the calculated error and the process is repeated till an acceptable error is obtained. The process

of obtaining the acceptable error is achieved using a back propagation learning procedure during the data training in a supervised learning environment. For the present work, the Levenberg–Marquardt training algorithm is employed and the errors in conjunction to the used training algorithm are computed in the form of mean square error (MSE), as given by Eq. (4), (Howard and Mark 2004). The performance of ANN model is assessed by statistical parameters such as coefficient of determination (R^2) (Arslan and Yetik 2014), given by Eq. (5) and root-mean-square error (RMSE) (Tugcu and Arslan 2017), given by Eq. (6), where Y_{output} is output value, $\overline{Y}_{output}$ is average output value, Y_{actual} is actual value, $\overline{Y}_{actual}$ is average output value, and n is the total number of data.

$$\text{RMSE} = \sqrt{\frac{\sum_{m=1}^{n}\left(Y_{m,output} - Y_{m,actual}\right)^2}{n}} \tag{5}$$

$$R^2 = \left[\frac{\sum_{m=1}^{n}\left(Y_{m,\text{output}} - \overline{Y}_{m,\text{output}}\right)\left(Y_{m,\text{actual}} - \overline{Y}_{m,\text{actual}}\right)}{\sqrt{\sum_{m=1}^{n}\left(Y_{m,\text{output}} - \overline{Y}_{m,\text{output}}\right)^2 \sum_{m=1}^{n}\left(Y_{m,\text{actual}} - \overline{Y}_{m,\text{actual}}\right)^2}}\right]^2 . \tag{6}$$

Results and discussion

Numerical dataset

For the development of the meta-model based on ANN, the results from the numerical simulations were utilized as the necessary dataset for the training of the ANN model. The numerical simulations of the airfoils have been carried out utilizing the validated computational case. The numerical simulation of each of the airfoil has been carried out for a range of Reynolds number ranging from 100,000 to 2,000,000 at an interval of 100,000 and over a range of angle of attack ranging from 0° to 20° at an interval of 2°. Thus for each airfoil, a total of 220 numerical simulations has

**Table 4** Performance of various ANN model with lift coefficient as output

ANN models	Neurons in hidden layer	Training		Testing	
		R^2	RMSE	R^2	RMSE
1	2	0.95412	0.04067	0.88915	0.05839
2	3	0.98761	0.01907	0.98431	0.02190
3	4	0.99389	0.01362	0.99551	0.01417
4	5	0.99803	0.00842	0.99644	0.00978
5	6	0.99818	0.00812	0.99639	0.01107
6	7	0.99813	0.00805	0.99697	0.00841
7	8	0.99806	0.00839	0.88702	0.01350
8	9	0.99929	0.00497	0.99879	0.00618

Table 5 Performance of various ANN model with drag coefficient as output

ANN models	Neurons in hidden layer	Training		Testing	
		R^2	RMSE	R^2	RMSE
1	2	0.95308	0.01414	0.93179	0.01753
2	3	0.99066	0.00658	0.99200	0.00539
3	4	0.99906	0.00202	0.99874	0.00201
4	5	0.99844	0.00254	0.99827	0.00298
5	6	0.99855	0.00234	0.99866	0.00247
6	7	0.99949	0.00149	0.99962	0.00146
7	8	0.99687	0.00352	0.99505	0.00469
8	9	0.99962	0.00124	0.99972	0.00124

been carried out. Prior to the development of meta-models for all the airfoils, the development of the meta-model for single airfoil, i.e., SV1 is carried out. Upon the successful development of the model for SV1 airfoil, the same topology of the ANN model is followed for the rest of the airfoils. Before using the numerical results for the training of the neural network for SV1 airfoil, all the numerical results of the SV1 airfoil were first randomly arranged, and a separate pool of 20 results was created for further testing and validation purpose. Thus with only 200 numerical results (70% for

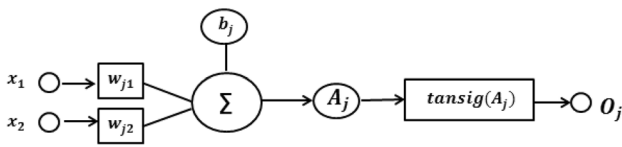**Fig. 5** Topology of the ANN model
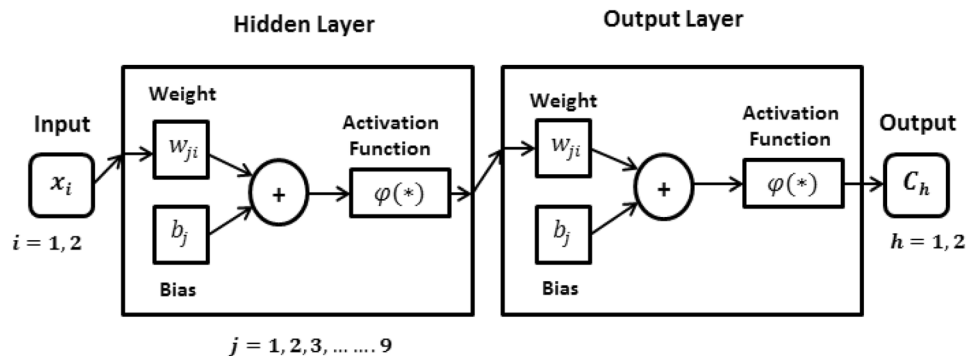
Fig. 6 Operational structure of neurons of the hidden layer

training, 15% for validation and 15% for testing), the development of various ANN models for SV1 airfoil was carried out. However, for the development of the ANN models for other airfoils, complete dataset with adequate pool distribution for training, validation, and testing is utilized. For the development of ANN models for other airfoils, the quota of dataset for validation and testing is increased to 20% and thus only 60% of 220 dataset is utilized for the training of the ANN models.

ANN model

The present ANN models are developed using the neural network toolbox of MATLAB®(R2015a) (2015). The ANN model utilizes a feed-forward network based on the back-propagation learning procedure. Out of the 200 CFD results, 140 data (70% data) were utilized for the training process, 30 data (15% data) were utilized for the validation process, and the remaining 30 data (15% data) were utilized for the testing process. The optimum number of neurons for the hidden layers was estimated by trial and error (Maleki et al. 2019). A total of nine ANN models were developed based on the number of the neurons (2–10) in the hidden layer. The performance of each of the model is characterized by the statistical parameters such as coefficient of determination (R^2) and root-mean-square error (RMSE). Table 4 and 5 show the statistical evaluations of the models for lift and drag coefficient, respectively. From Table 4, it can be observed that the ANN model with nine neurons in the hidden layer has maximum R^2 of 0.99929 and 0.99879 for training and testing dataset and minimum RMSE of 0.00497 and 0.00618 for training and testing dataset, respectively. Similarly, from Table 5, it can be observed that the ANN model with nine neurons in the hidden layer has maximum R^2 of 0.99962 and 0.99972 for training and testing dataset and minimum RMSE of 0.00124 and 0.00123 for training and testing dataset, respectively. Hence, the optimal ANN model is framed as input with two input variables ($i = 1, 2$), hidden layer with nine neurons ($j = 1, 2, 3, … 9$), and output layer with two neurons ($h = 1, 2$) for the two output parameters. The topology of the ANN model is shown in Fig. 5. The output parameter $\left(C_h\right)$ is evaluated by using Eqs. (7)–(10).

The input $\left(A_j\right)$ to the neuron (j) of the first hidden layer is given by Eq. (7), whereas the output $\left(O_j\right)$ of neuron (j) from the hidden layer is given by Eq. (8). The operational structure of the neurons at the hidden layer is shown in Fig. 6. The

Table 6 Associated weight and bias of the hidden layer

Neuron (j)	Neurons of the hidden layer								
	1	2	3	4	5	6	7	8	9
Weights (w_{ji})									
w_{j1}	−0.0582	−0.1877	−0.9098	0.9058	0.4411	3.6643	−0.0445	0.2739	−0.6410
w_{j2}	−6.1922	−3.6667	4.0398	−1.8932	−0.5069	0.1902	−1.3511	−1.7571	1.4176
Bias (b_j)	−7.0401	3.6732	2.6070	−0.8746	1.0827	5.0301	0.3008	0.6220	2.1116

Fig. 7 Operational structure of
neurons of the output layer
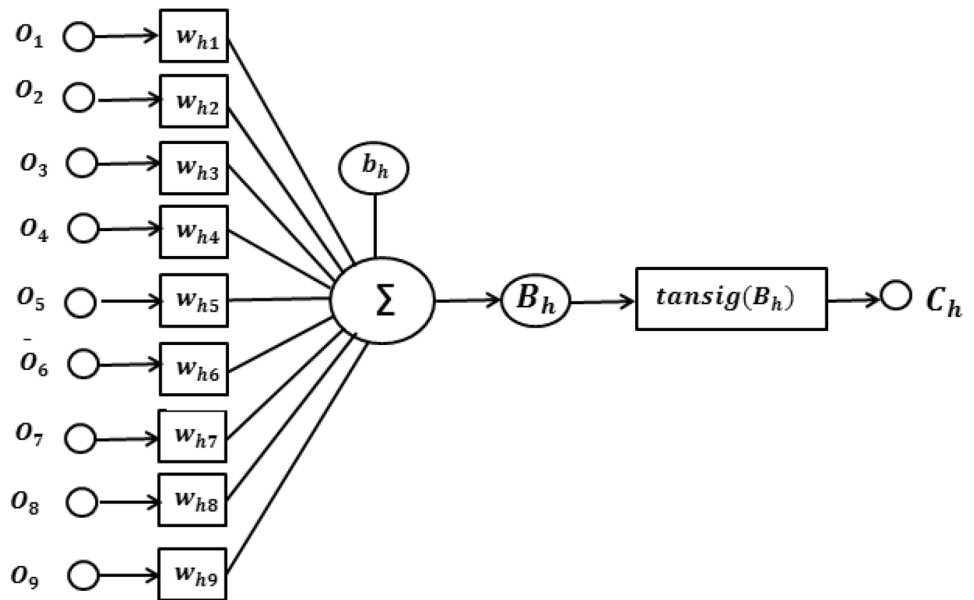
associated weights (w_{ji}) and bias (b_j) of neurons of the hidden layer is shown in Table 6.

$$A_j = \sum_{i=1}^{2} x_i w_{ji} + b_j \tag{7}$$

$$O_j = \frac{2}{1 + e^{-2A_j}} - 1 \tag{8}$$

Now, the input (B_h) to the neuron h of the output layer is given by Eq. (9), whereas the output (C_h) of the neuron h from the second hidden layer is given by Eq. (10). The operational structure of the neurons at the output layer is shown in Fig. 7. The associated weights (w_{hj}) and bias (b_h) of neurons of the output layer is shown in Table 7.

$$B_h = \sum_{j=1}^{9} O_j w_{hj} + b_h \tag{9}$$

$$C_h = \frac{2}{1 + e^{-2B_h}} - 1 \tag{10}$$

The predicted lift and drag coefficient outputs from the ANN model were compared with the separate pool of data that were kept aside earlier and had not contributed to the development of the ANN model. Table 8 shows the separate pool for data and its comparison with the ANN outputs. Figures 8a and 9a show the predicted lift and drag coefficient for

Table 7 Associated weights and bias of the output layer

Neuron (h)	Neurons of the output layer	
	1	2
Weights (w_{hj})		
w_{h1}	− 1.373	0.6648
w_{h2}	− 0.159	− 0.2895
w_{h3}	0.6384	0.5264
w_{h4}	1.1014	− 0.1301
w_{h5}	− 3.283	− 0.7093
w_{h6}	4.0987	− 2.3709
w_{h7}	− 4.404	− 0.7533
w_{h8}	3.6444	0.0899
w_{h9}	− 2.383	0.3058
Bias (b_h)	− 4.686	3.0237

SV1 airfoil from the ANN model in comparison with actual CFD results for the separate pool of data. A high coefficient of determination with 0.99632 and 0.99934, and low root-mean-square error of 0.01332 and 0.00164 for the predicted lift and drag coefficient suggests the capabilities of the ANN model to predict the performance of the airfoil at different operating conditions.

With the similar topology of the ANN model, the ANN models for the rest of the airfoils are also developed. Figure 8b–f shows the comparison of the ANN predicted lift coefficient and CFD lift coefficient for test dataset comprising of 20% of the dataset which has not been utilized in the development of the ANN model. Similarly, Fig. 9b–f shows

Table 8 A comparison of the predicted outputs from ANN model with the separate pool of test data

| Reynolds number	Angle of attack	Coefficient of lift		Coefficient of drag	
		Actual	ANN predicted	Actual	ANN predicted
1,500,000	2	0.906	0.9052	0.0181	0.0176
1,000,000	18	1.0977	1.1183	0.174	0.1723
100,000	10	0.8266	0.8347	0.1079	0.1088
100,000	0	0.5401	0.5683	0.0309	0.0289
1,100,000	14	1.2123	1.1962	0.1066	0.1081
1,000,000	20	1.0912	1.1053	0.2073	0.2099
800,000	0	0.6854	0.6846	0.0181	0.0185
1,700,000	2	0.9127	0.9107	0.0177	0.0174
2,000,000	4	1.098	1.0766	0.0203	0.0182
600,000	6	1.0664	1.0476	0.0388	0.0415
600,000	14	1.0933	1.0930	0.1203	0.1198
1,900,000	4	1.0951	1.0773	0.0205	0.0185
1,900,000	16	1.2614	1.2668	0.1241	0.1229
1,700,000	16	1.2407	1.2467	0.1267	0.1254
2,000,000	14	1.3067	1.2922	0.095	0.0959
1,900,000	2	0.9184	0.9150	0.0174	0.0173
300,000	6	0.9478	0.9540	0.0493	0.0496
1,200,000	0	0.7038	0.7048	0.0167	0.0180
900,000	6	1.1332	1.1151	0.0332	0.0370
1,500,000	20	1.1623	1.1579	0.1973	0.1981
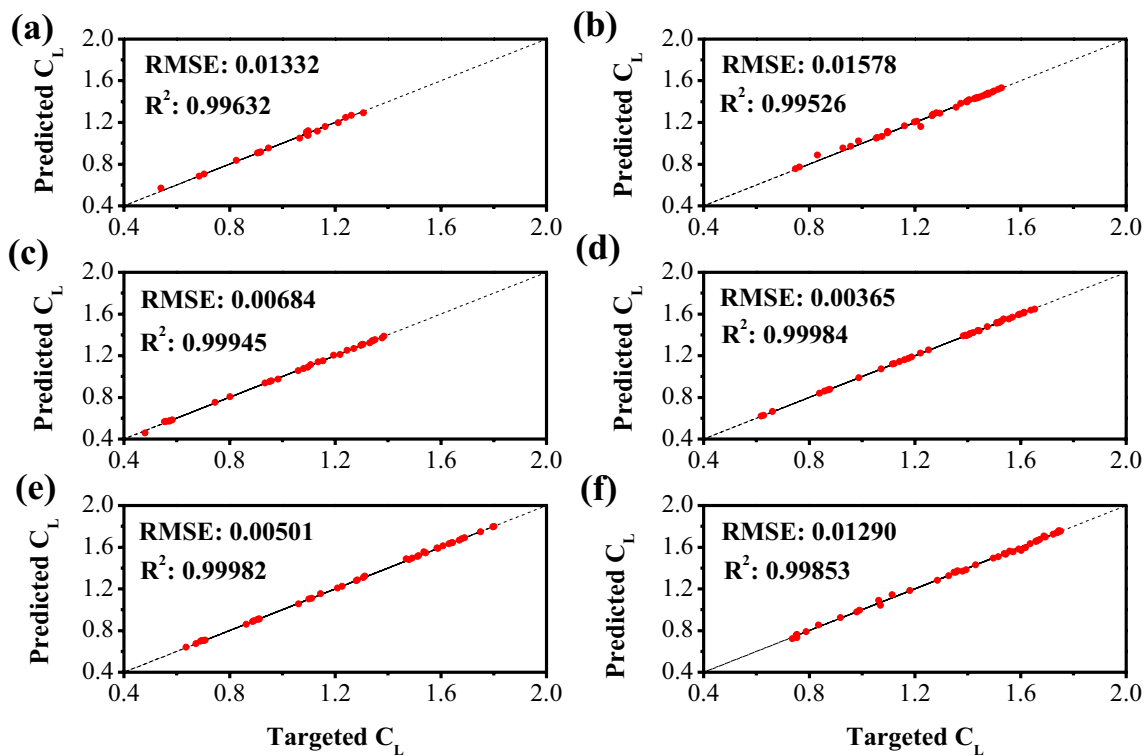
Fig. 8 Predicted lift coefficient from ANN models versus targeted lift coefficient from numerical simulations for the test dataset for **a** SV1, **b** SV2, **c** SV3, **d** SV4, **e** SV5, and **f** SV6
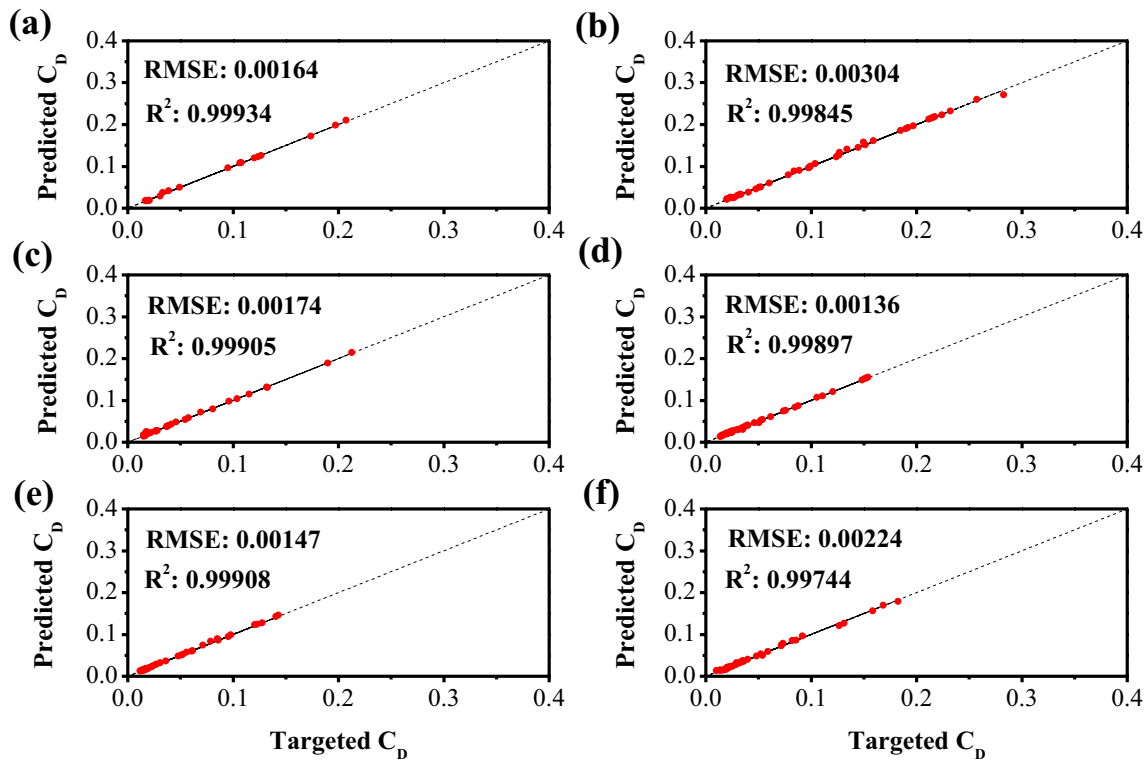
Fig. 9 Predicted drag coefficient from ANN models versus targeted drag coefficient from numerical simulations for the test dataset for **a** SV1, **b** SV2, **c** SV3, **d** SV4, **e** SV5, and **f** SV6

the comparison of the ANN predicted drag coefficient and CFD predicted drag coefficient for the test dataset. A high value of coefficient of determination and low root-mean-square error for the predicted lift and drag coefficient suggests the effective capability of the developed ANN models.

Figures 10 and 11 shows the variation of lift and drag coefficient with angle of attack for a range of Reynolds number, obtained by the ANN-based models and CFD simulations, respectively. From Figs. 10 and 11, it can be observed that for any given airfoil, even at higher angles of attack where the nonlinear characteristics are predominant, the ANN-based models had sufficiently predicted the results with a reasonable degree of accuracy. This characteristic of ANN model is also consistent at different Reynolds number. This indicates not only the capability of the ANN model to effectively model the highly nonlinear characteristics but also suggests a general topology of the ANN model for predicting the lift and drag coefficient at any given Reynolds number and angle of attack from a predefined range.

The aerodynamic design of wind turbine rotor needs to be appropriately adjusted on account of change in airfoil database because of different Reynolds number consideration (Ge et al. 2016). The flexibility to accommodate for the

variation of Reynolds number, which had not traditionally accounted by the analytical or semi-empirical mathematical models, is achieved through ANN-based models. Thus, the ANN-based models can be effectively utilized in the blade element momentum theory and the aerodynamic characteristics of the airfoil can be obtained at local Reynolds number instead of an approximated Reynolds number and hence reducing the uncertainty on account of inadequate consideration of Reynolds number on integrated design and performance evaluation of wind turbine.

Conclusion

The development of ANN-based meta-models has been carried out to predict the lift and drag coefficient of the in-house developed airfoils, namely SV1, SV2, SV3, SV4, SV5, and SV6 for a given range of Reynolds number (100,000–2,000,000) and angle of attack (0°–20°). The training dataset for the development of the ANN models has been obtained by the numerical simulation of each of the airfoils for the given range of Reynolds number at an interval of 100,000 and also at the given range of angle of attack at
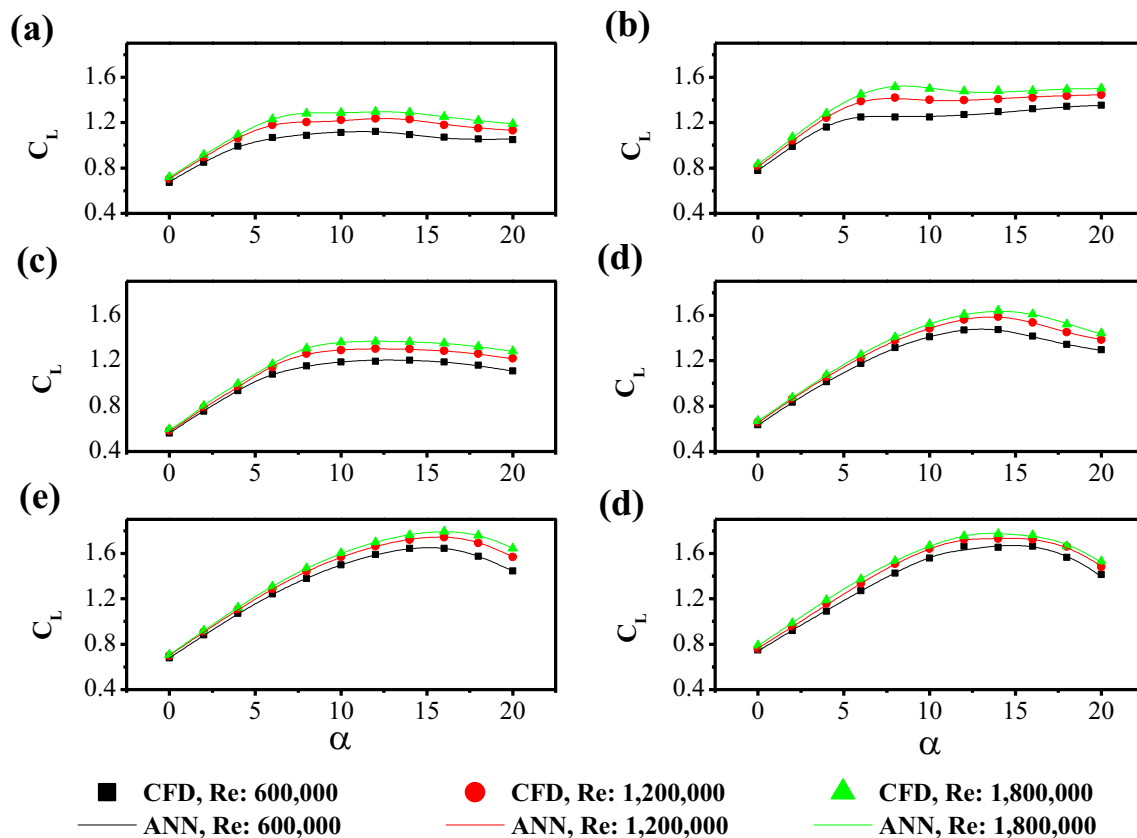
Fig. 10 Variation of lift coefficients with the angle of attack obtained from ANN models and CFD results over a range of Reynolds number for **a** SV1, **b** SV2, **c** SV3, **d** SV4, **e** SV5, and **f** SV6

an interval of 2°. Prior to the development of ANN models for all the given airfoils, initially, an ANN model for only SV1 is developed. Upon the successful development of the ANN model for the SV1 airfoil with coefficient of determination of 0.99632 and 0.99934 for lift and drag coefficient, respectively, for a separate pool of random data which has not been utilized in the model development, the topology of the developed ANN model has been adopted for the development of rest of the ANN models. With a testing dataset comprising of 20% of the randomly arranged overall dataset, high coefficient of determination and low root-mean-square

error for lift and drag coefficient for all the airfoil suggest an effective topology of general ANN model for predicting lift and drag coefficient of an airfoil for a given range of Reynolds number and angle of attack. Upon comparing the variation of ANN predicted lift and drag coefficient with angle of attack for a range of Reynolds number with the CFD results for all the airfoils, the capabilities of the ANN model to effectively model highly nonlinear aerodynamic characteristics of airfoils was also observed.
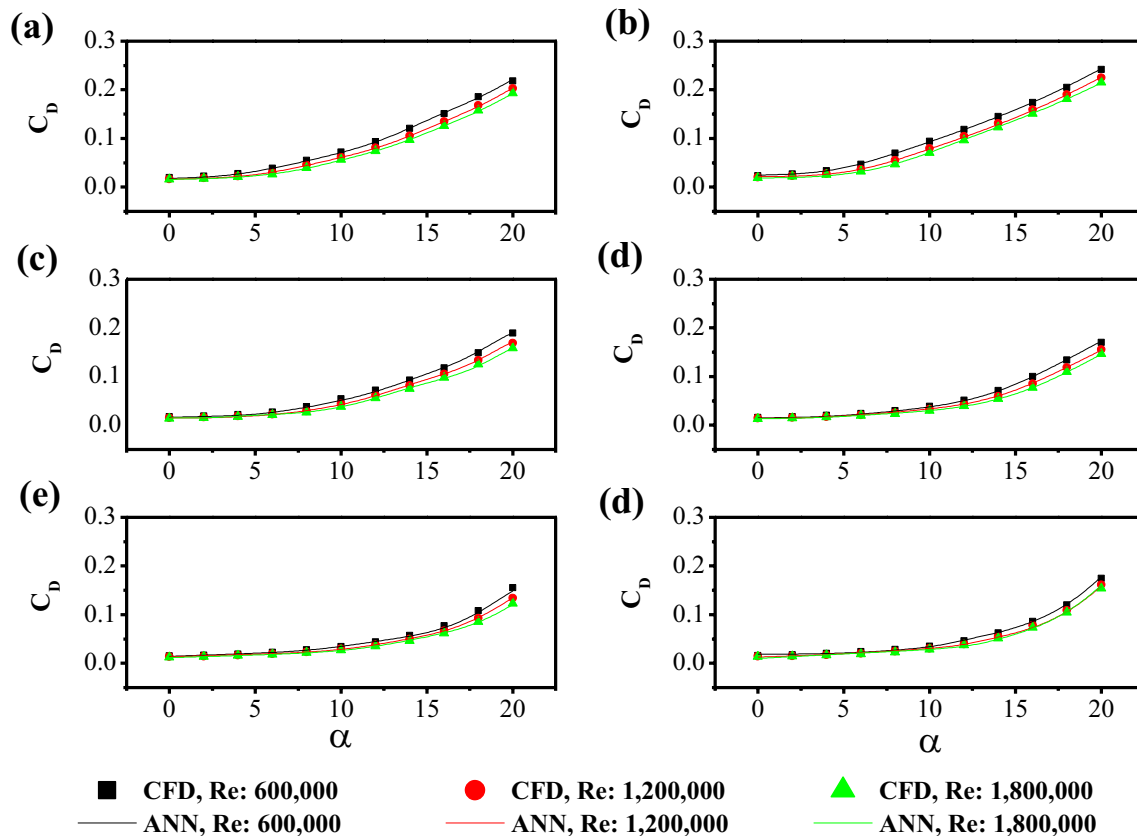
Fig. 11 Variation of drag coefficients with the angle of attack obtained from ANN models and CFD results over a range of Reynolds number for **a** SV1, **b** SV2, **c** SV3, **d** SV4, **e** SV5, and **f** SV6

Declarations

Conflict of interest The authors declare that they have no conflict of interest.

References

Ansys I (2015) ICEM CFD theory guide. Ansys Inc

Ansys I (2013) ANSYS fluent theory guide (release 15.0). Canonsburg, PA

Arslan O, Yetik O (2014) ANN modeling of an orc-binary geothermal power plant: Simav case study. Energy Sources, Part A Recover Util Environ Eff 36:418–428. https://doi.org/10.1080/15567036.2010.542437

Bai C-J, Chen P-W, Wang W-C (2016) Aerodynamic design and analysis of a 10 kW horizontal-axis wind turbine for Tainan. Taiwan Clean Technol Environ Policy 18:1151–1166. https://doi.org/10.1007/s10098-016-1109-z

Bai CJ, Wang WC (2016) Review of computational and experimental approaches to analysis of aerodynamic performance in horizontal-axis wind turbines (HAWTs). Renew Sustain Energy Rev 63:506–519. https://doi.org/10.1016/j.rser.2016.05.078

Bai CJ, Wang WC, Chen PW (2017) Experimental and numerical studies on the performance and surface streamlines on the blades of a horizontal-axis wind turbine. Clean Technol Environ Policy 19:471–481. https://doi.org/10.1007/s10098-016-1232-x

Bavanish B, Thyagarajan K (2013) Optimization of power coefficient on a horizontal axis wind turbine using bem theory. Renew Sustain Energy Rev 26:169–182. https://doi.org/10.1016/j.rser.2013.05.009

Behera SK, Meher SK, Park HS (2015) Artificial neural network model for predicting methane percentage in biogas recovered from a landfill upon injection of liquid organic waste. Clean Technol Environ Policy 17:443–453. https://doi.org/10.1007/s10098-014-0798-4

Belamadi R, Djemili A, Ilinca A, Mdouki R (2016) Aerodynamic performance analysis of slotted airfoils for application to wind turbine blades. J Wind Eng Ind Aerodyn 151:79–99. https://doi.org/10.1016/j.jweia.2016.01.011

Ceyhan Ö (2012) Towards 20MW wind turbine: High reynolds number effects on rotor design. In: 50th AIAA aerospace sciences meeting including the new horizons forum and aerospace exposition, pp 9–12. https://doi.org/10.2514/6.2012-1157

Chakraborty S, Chowdhury S, Das SP (2013) Artificial neural network (ANN) modeling of dynamic adsorption of crystal violet from aqueous solution using citric-acid-modified rice (Oryza sativa) straw as adsorbent. Clean Technol Environ Policy 15:255–264. https://doi.org/10.1007/s10098-012-0503-4

Chattot JJ (2003) Optimization of wind turbines using helicoidal vortex model. J Sol Energy Eng Trans ASME 125:418–424. https://doi.org/10.1115/1.1621675

El-Okda YM (2015) Design methods of horizontal axis wind turbine rotor blades. Int J Ind Electron Drives 2:135. https://doi.org/10.1504/ijied.2015.072789

Ge M, Fang L, Tian D (2015) Influence of reynolds number on multi-objective aerodynamic design of a wind turbine blade. PLoS ONE 10:1–25. https://doi.org/10.1371/journal.pone.0141848

Ge M, Tian D, Deng Y (2016) Reynolds number effect on the optimization of a wind turbine blade for maximum aerodynamic efficiency. J Energy Eng. https://doi.org/10.1061/(ASCE)EY.1943-7897.0000254

Gue IHV, Ubando AT, Tseng ML, Tan RR (2020) Artificial neural networks for sustainable development: a critical review. Clean Technol Environ Policy 22:1449–1465. https://doi.org/10.1007/s10098-020-01883-2

Hand MM et al (2001) Unsteady aerodynamics experiment phase VI: wind tunnel test configurations and available data campaigns. Golden, CO (US)

Hassanzadeh A, Hassanzadeh Hassanabad A, Dadvand A (2016) Aerodynamic shape optimization and analysis of small wind turbine blades employing the Viterna approach for post-stall region. Alex Eng J 55:2035–2043. https://doi.org/10.1016/j.aej.2016.07.008

Howard D, Mark B (2004) Neural network toolbox documentation. Neural Netw Tool 2004:846

Lanzafame R, Messina M (2007) Fluid dynamics wind turbine design: critical analysis, optimization and application of BEM theory. Renew Energy 32:2291–2305. https://doi.org/10.1016/j.renene.2006.12.010

Leishman JG (2006) Principles of helicopter aerodynamics

Maleki H, Sorooshian A, Goudarzi G et al (2019) Air pollution prediction by using an artificial neural network model. Clean Technol Environ Policy 21:1341–1352. https://doi.org/10.1007/s10098-019-01709-w

MATLAB (2015) R2015a. The MathWorks Inc., Natick, Massachusetts

McGhee R, Walker B, Millard B (1988) Experimental results for the eppler 387 airfoil at low reynolds numbers in langley low-turbulence pressure tunnel. Nasa 4062:238

McTavish S, Feszty D, Nitzsche F (2013) Evaluating Reynolds number effects in small-scale wind turbine experiments. J Wind Eng Ind Aerodyn 120:81–90. https://doi.org/10.1016/j.jweia.2013.07.006

Miller MA, Kiefer J, Westergaard C et al (2019) Horizontal axis wind turbine testing at high Reynolds numbers. Phys Rev Fluids 4:1–22. https://doi.org/10.1103/PhysRevFluids.4.110504

Pinkerton RM (1936) Calculated and measured pressure distributions over the midspan section of the NACA 4412 airfoil. 563

Reggio M, Villalpando F, Ilinca A (2011) Assessment of turbulence models for flow simulation around a wind turbine airfoil. Model Simul Eng. https://doi.org/10.1155/2011/714146

Tangler JL, Somers DM (1995) NREL Airfoil Families for HAWTs. Golden, CO.(US)

Tugcu A, Arslan O (2017) Optimization of geothermal energy aided absorption refrigeration system—GAARS: a novel ANN-based approach. Geothermics 65:210–221. https://doi.org/10.1016/j.geothermics.2016.10.004

Wallach R, de Mattos BS, da Mota Girardi R (2006) Aerodynamic coefficient prediction of a general transport aircraft using neural network. In: ICAS Secretariat 25th congress of the international council of the aeronautical science, vol 2, pp 1199–1214. https://doi.org/10.2514/6.2006-658

Wang L, Tang X, Liu X (2012) Optimized chord and twist angle distributions of wind turbine blade considering Reynolds number effects

Zhu WJ, Shen WZ, Sørensen JN (2014) Integrated airfoil and blade design method for large wind turbines. Renew Energy 70:172–183. https://doi.org/10.1016/j.renene.2014.02.057